processes

MDPI

Article

Influence of Brown's Gas on Cracking Behavior of Gas-Phase Tar during Pine Wood Pyrolysis

Shuo Yang *, Yudong Fu *, Jie Cui, Zhanzhi Liu *, Daocheng Qin, Lin Xu and Youning Xu

Key Laboratory of Liaoning Province for Clean Combustion Power Generation and Heating Technology, Shenyang Institute of Engineering, Shenyang 110136, China; cuicuijiejie25@163.com (J.C.); qdc850649712@163.com (D.Q.); lin_xu1989@163.com (L.X.); 49784322@163.com (Y.X.)

* Correspondence: ys_yang_shuo@163.com (S.Y.); fu_yudong@126.com (Y.F.); liuzhanzhi0215@163.com (Z.L.); Tel.: +86-24-3197-5545 (S.Y.)

Abstract: The effect of Brown's gas on the gas-phase tar cracking behavior, carbonic oxide (CO) production rate, and gaseous product temperature during the pine wood pyrolysis was preliminarily explored. By the application of cold trapping and gravimetric methods, it was found that Brown's gas reduces the energy barrier of thermochemical conversion for gas-phase tar, widens the temperature range of gas-phase tar accelerated cracking, and increases the cracking rate. When the pyrolysis temperature increases by 1 °C, the average cracking rate of gas-phase tar increases from C = 4.58 g·Nm^{-3} (flow volume ratio of Brown's gas to nitrogen, $X_{(Brown's\ gas)}$:N_2 = 0%) to C = 4.8 g·Nm^{-3} (X:N_2 = 1%) and C = 5.02 g·Nm^{-3} (X:N_2 = 5%). While participating in the deep cracking of gas-phase tar, Brown's gas reduces the conversion energy barrier of the gas-phase tar to CO. The CO production rate rises from the initial 1.87% (X:N_2 = 0%) to 4.22% (X:N_2 = 1%) and 5.52% (X:N_2 = 5%) per 1 °C of increased pyrolysis temperature. The consumption of Brown's gas is 0.32 m^3 per 1 g·Nm^{-3} of gas-phase tar cracking within the pyrolysis residence time of 30 min.

Keywords: Brown's gas; biomass pyrolysis; gas-phase tar

Citation: Yang, S.; Fu, Y.; Cui, J.; Liu, Z.; Qin, D.; Xu, L.; Xu, Y. Influence of Brown's Gas on Cracking Behavior of Gas-Phase Tar during Pine Wood Pyrolysis. *Processes* **2022**, *10*, 1231. https://doi.org/10.3390/pr10071231

Academic Editors: Francesca Raganati and Alessandra Procentese

Received: 3 June 2022
Accepted: 16 June 2022
Published: 21 June 2022

1. Introduction

Hydrogen energy refers to the chemical energy released by hydrogen combustion, that is, hydrogen reacting with oxygen to generate water and release heat [1]. Hydrogen and oxygen can be directly converted into electrical energy within the fuel cell [2], or as an intermediate carrier of heat and mechanical energy to achieve energy conversion [3]. However, there are still many potential hydrogen energy application characteristics and scenarios that have not been fully explored, among which Brown's gas as a hydrogen-rich mixed gas is popular with inventors and hobbyists worldwide. The researchers used the dry or wet cell [4–7] to produce a mixture of hydrogen and oxygen gas known by various names such as HHO, hydroxy, oxyhydrogen, and Brown's gas. The properties of this mixture show surprising. For example, Brown's gas exhibits a cool flame (~130 °C), yet it can vaporize tungsten, a feat beyond today's commercial welding torches. The radioactivity of americium can be changed by the Brown's gas flame [8]. The academic community has yet to explore or explain this. In recent years, enabling efficient use of Brown's gas in selected engineering applications (transportation and sustainable power generation) has been introduced by some comprehensive reviews [9,10].

The usage of fossil fuel and the resulting drastic increase in pollution levels has made us realize the need for a new sustainable fuel which does not cause pollution and climate change. Using Brown's gas as a fuel enhancer in internal combustion engines, there is a net increase in brake power ranging from 2% to 5.7% and an increase in brake thermal efficiency which ranges from 10.26% to 34.9%. A decrease in specific fuel consumption is observed from 20% to 30% along with a decrease in CO and HC emissions on an average of 18% and 14%, respectively [11]. Gad et al. [12] explored the emissions and performance

study of diesel engine using cotton ethyl ester blend enriched with HHO gas and kerosene additives. HHO gas with kerosene blends accompanied by ethyl ester cotton oil lessens the brake specific fuel consumption and increases the brake thermal efficiency by 17% and 26.2%, respectively. HHO enriching is favorable in the combustion characteristics improvement. Gad et al. [13] performed performance, combustion characteristics and emissions investigations of diesel engines using HHO gas from dry and wet cells. HHO gas addition enhances the brake thermal efficiency by 2% and 2.5% but the exhaust gas temperature highest decreases for dry and wet cells are 8 and 10%. Liu et al. [14] investigated the combustion stability of shale gas engines by adjusting the HHO blending ratio. In particular, the influence of HHO content on the in-cylinder pressure and heat release process of a shale gas engine was analyzed, the combustion cycle trends were discussed, and the dynamic characteristics of the combustion process were evaluated. The influence of HHO content on the stability of the flame propagation process in the cylinder was then determined.

A research team from Yonsei University vitrified municipal solid waste incinerator (MSWI) fly and bottom ashes at 1450 °C by using Brown's gas, for the first time [15–17]. It was further confirmed that fly and bottom ashes contained crystalline contents which transformed into amorphous glassy structure on vitrification. As the vitrified ash product of bottom ash and its mixture with fly ashes were found to be non-hazardous, they could be considered as construction and road building material. Min et al. [18] melted four types of waste asbestos containing material such as spread asbestos, plasterboard asbestos, slate asbestos, and asbestos 99 wt%, in a melting fumace at 1450–1550 °C that uses a mixture of hydrogen and oxygen (Brown's gas) as a fuel. It was further confirmed by SEM and XRD studies that all waste materials contained some crystalline structures which transformed into amorphous glassy structure on melting. Wang et al. [19] investigated the combined effects of HHO gas with other fuels, including coal and oil. The combinations of HHO with coal and oil can improve the efficiency of electricity generation while reducing the pollution. Specifically, the addition of 1 kg HHO gas with Indian lignite can improve efficiency by 0.2%. Kenanolu et al. [20] investigate how to compensate for the drawbacks of using ammonia as the main fuel in a gas turbine by hydrogen and hydroxy-gas enrichment. During the experiments, propane that is standard working fuel of the gas turbine, neat ammonia, as well as a 10 L/min ammonia fuel enriched with 3 L/min, 5 L/min, and 7 L/min hydroxy gas, were utilized. NOx emissions should be kept under control in addition to the increase in the performance and elimination of the carbon emissions. Gu et al. [21] developed a medium-sized hydrogen and oxygen (HHO) generator, with high energy conversion rate and adjustable output gas. The HHO gas was then introduced into a biomass hot air generator for mixed combustion. The average concentrations of CO, NO and smoke decreased by 93.0%, 22.5% and 80%, respectively. Integration of biomass fuel and HHO gas can effectively reduce pollutant emissions and save fuel. Nabil et al. [22] proposed that HHO can be used as a substitute fuel for LPG which is used for cooking applications in villages and remote locations.

In summary, compared with the research on the welding and internal combustion engine co-firing, Brown's gas has less research in the fields of direct combustion power generation and clean heating (gas turbine, biomass boiler, and waste incineration power generation) [22]. The research on the mechanism of Brown's gas participating in the biomass combustion and its catalysis effect for gas-phase tar are not deep enough. In this paper, numerical analysis has been conducted for the main composition changes of gas phase tar in the atmosphere of Brown' gas, and the effect of Brown's gas on the gas-phase tar, CO, and gaseous product temperature is quantitatively studied by experimental means. In particular, under mild condition (lower pyrolysis temperature or without catalyst), the cracking rule of biomass gas-phase tar by Brown' gas is described. As Brown's gas is a compound gas, the pyrolysis atmosphere in this paper belongs to an oxygen-deficient pyrolysis environment rich in hydrogen and free radicals.

2. Numerical Investigation

2.1. Numerical Methods and Boundary Conditions

In this paper, based on the Cantera open-source program, the effect of Brown's gas on gas-phase tar in the biomass pyrolysis has been preliminarily determined. According to the division of tar components in gaseous products at different temperatures, the benzene (C_6H_6), toluene ($C_6H_5CH_3$), phenol (C_6H_5OH), xylene ($CH_3C_6H_5CH_3$), and methylnaphthalene ($C_{10}H_7CH_3$) were chosen as representative constituents in gas-phase tar, as shown from Tables A1–A5 in the Appendix A.

Brown's gas is a mixture of gases produced by the alkaline solution (KOH) electrolysis in this experiment. Its main components are hydrogen (H_2) and oxygen (O_2) (H_2 accounts for 60.12%, O_2 accounts for 29.87%). In addition, there are small amounts of water vapor and active radicals such as -H, -OH, and -O. In this experiment, the 83 mole Brown's gas can be electrolyzed from one L KOH solution (calculated according to the Clapeyron equation [23]). The ratio of hydrogen, oxygen, and the other radical ions is H_2:O_2:x = 2:1:1 in the Brown's gas, and the initialization parameters of Brown's gas are shown in Table 1.

Table 1. Brown's gas parameters in numerical calculation.

Element	H_2	O_2	H	H_2O(g)	OH	O
Initial value (mol)	4.15×10^{-2}	2.075×10^{-2}	5.18×10^{-3}	5.18×10^{-3}	5.18×10^{-3}	5.18×10^{-3}
Normalization (-)	8.16×10^{-3}	4.08×10^{-3}	1.02×10^{-3}	1.02×10^{-3}	1.02×10^{-3}	1.02×10^{-3}

The pyrolysis temperature directly affects the gas-phase tar content and the gaseous products. The range of pyrolysis temperature is from 600.15 °C to 1000.15 °C in the numerical simulation. A transient reaction system was built, and the initial content of gas-phase tar was set to 1 mole. The heating rate is 10 °C/min. The other parameters include initial temperature (T = 25 °C) and response time (t = 30 min). Ambient atmosphere is nitrogen.

2.2. Discussion

As shown in Figure 1, the C_6H_5OH first started to crack at T = 1020.2 K in the absence of Brown's gas with the increasing temperature, and there were no obvious changes of the other gas-phase tar components. When the temperature was up to T = 1100 K, other gas-phase tar components showed a cracking trend. At the same time, the C_6H_5OH is more sensitive to temperature, and its cracking is accelerated with the increasing temperature. When the temperature was up to T = 1162.7 K, the other gas-phase tar components except phenol (C_6H_5OH) began to accelerate the cracking. From the Figure 2, the onset cracking temperature of each gas-phase tar component was lessened under the effect of Brown's gas, and the gas-phase tar began to have a weak cracking trend at the temperature of T = 892.5 K. Compared with the condition without introduced Brown's gas, the cracking rate of C_6H_5OH with the increasing temperature was still the fastest. When the temperature was T = 1130.5 K, each gas-phase tar component began to accelerate cracking. Therefore, the Brown's gas lessens the onset temperature of gas-phase tar cracking to varying degrees.

By calculating the content of gas-phase tar in the final state (see Figure 3), compared with the condition without introduced Brown's gas, the cracking rate of $C_6H_5CH_3$ content was the largest, $M_{(C6H5CH3)}$ = 3.51%, (M = ($M_{\text{Brown'gas}} - M_{\text{no Brown' gas}}$)/$M_{\text{Brown'gas}}$). The cracking rate of the other gas-phase tar components was $M_{(C6H6)}$ = 0.94%, $M_{(C6H5OH)}$ = 1.90%, $M_{(C10H7CH3)}$ = 3.34%, and $M_{(CH3C6H5CH3)}$ = 2.04%, respectively. Therefore, Brown's gas plays a significant role in promoting the cracking of $C_6H_5CH_3$ and $C_{10}H_7CH_3$, and has a relatively weak effect on C_6H_6 cracking. In summary, the numerical study shows that Brown's gas reduces the activation temperature required for gas-phase tar cracking. On the other hand, it accelerates the catalytic cracking rate of gas-phase tar. Therefore, it is necessary to further carry out experimental research on the catalytic cracking behavior of Brown's gas on gas-phase tar in the biomass pyrolysis.

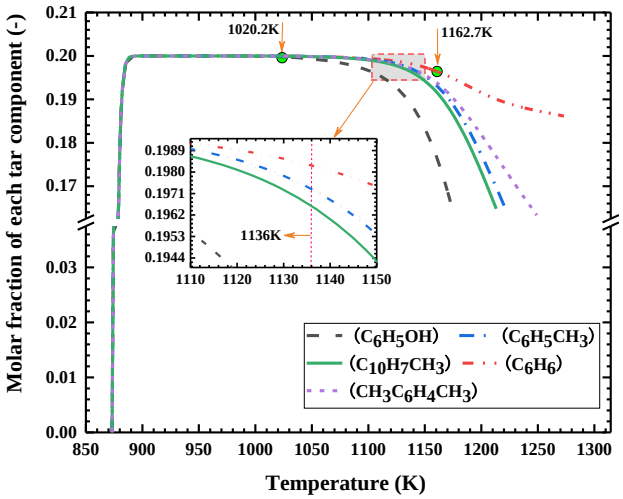

Figure 1. Variation of gas-phase tar with temperature without introduced Brown's gas.

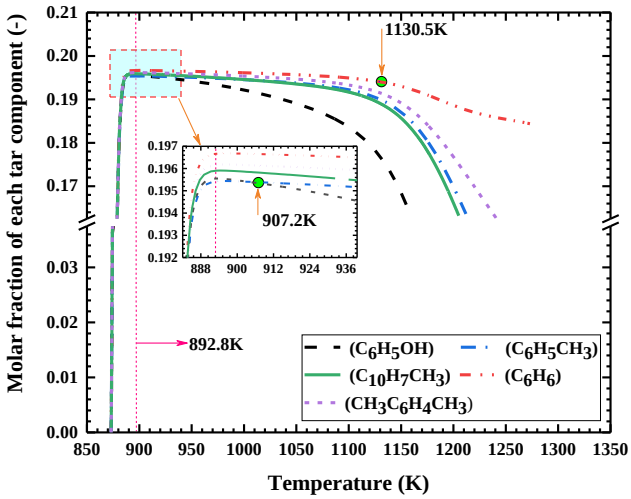

Figure 2. Variation of gas-phase tar with temperature with introduced Brown's gas.

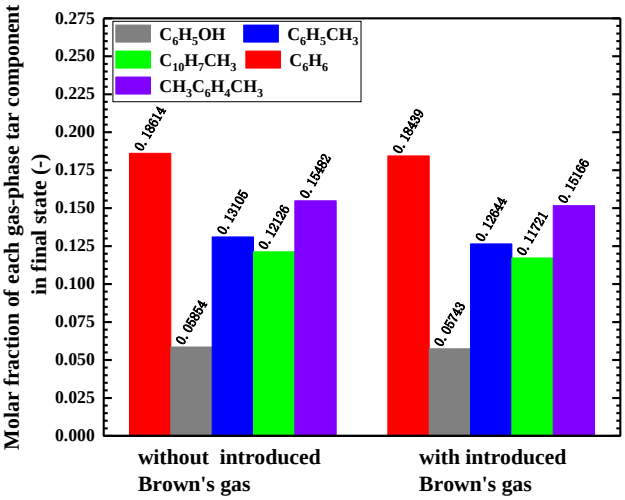

Figure 3. The molar fraction of each gas-phase tar component in the final state of reaction 3. Experiment research.

3. Experiment Research

3.1. Materials and Methods

3.1.1. Thermogravimetric Experiment

The experimental platform includes a Brown's gas generation system, a gas distribution system, a fixed bed tube furnace pyrolysis device, and a tar cold trapping system (see Figure 4). In this paper, the cold trapping method (CTM) was used to capture the gas-phase tar in the biomass pyrolysis process. This method is widely used by scholars in China and abroad, and it is mainly based on the low temperature condensation characteristic of gas-phase tar. The tar gravimetric method is adopted for the quantitative analysis. The principle is that the tar is dissolved in dichloromethane to form a sample solution, then the sample solution is placed in a constant temperature water bath at 75 °C for distillation, and the tar finally is weighed.

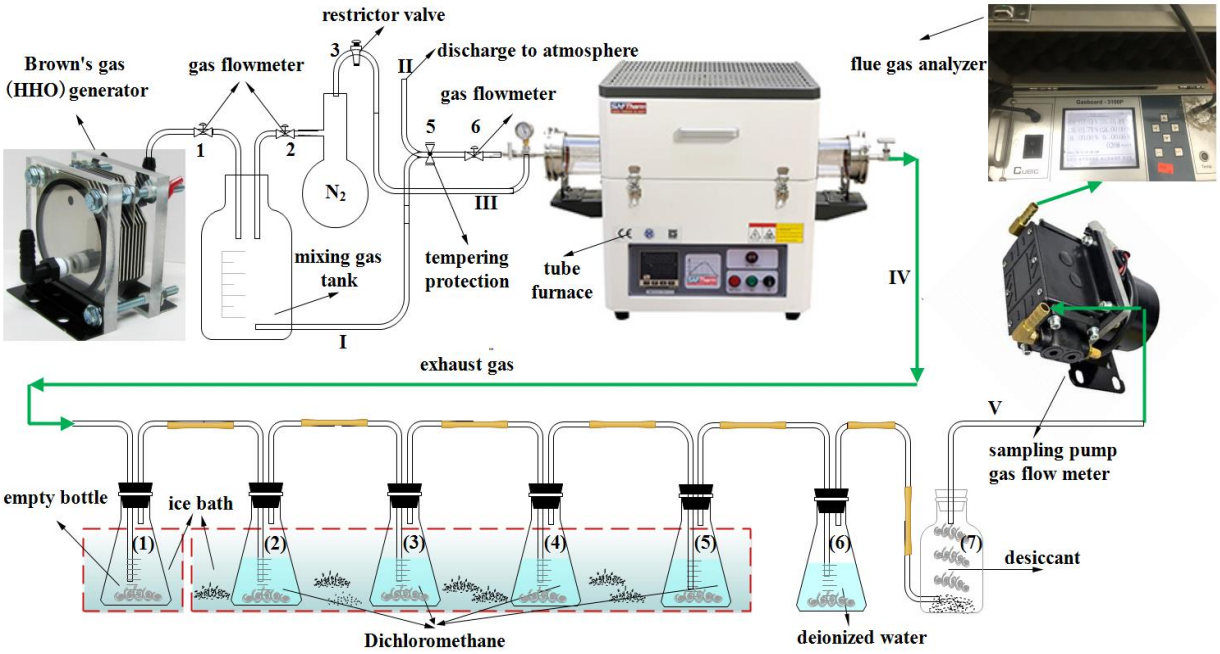

Figure 4. Experimental system for gas-phase tar cold trapping during the biomass pyrolysis (I, II, III, IV, and V represent gas path, respectively).

The experimental platform includes the following equipment, Brown's gas generator (KOH electrolyte, the rated gas production is 1.1 L/min), fixed-bed tube furnace (heating range is 300 °C~1200 °C, the optimal heating rate is less than or equal to 10 °C/min, maximum heating rate is 20 °C/min, and heating zone length is 200 mm), flue gas analyzer, sampling pump (volume flow rate is 0.2 L/min–4 L/min, ±5%), gas mixing tank with three-holes, gas flow meter (measuring range of N_2 flowmeter: 0.1 L/min~1.5 L/min), and several anti-backfire valves and throttles. The parameters of the thermogravimetric analyzer are as follows. Heating temperature is from 23 °C to 1450 °C. Heating rate is from 0.1 to 100 °C/min. Temperature sensitivity is 0.1 °C. Thermogravimetric range is 1–200 mg. Thermogravimetric sensitivity is 0.1 μg.

Pine wood was selected as the biomass pyrolysis raw material in the experiment. The elemental and proximate analysis were performed on the pine wood particles before the experiment. The results are shown in Tables 2 and 3. According to the data in Table 2, it can be seen that the content of carbon, hydrogen, and oxygen in pine wood particle is relatively high, accounting for more than 90%. Hydrogen exists mainly in the form of hydrocarbons in biomass. As shown in Table 3, the ash content is low and the volatile fraction content is high, indicating that the more organic hydrocarbons in the volatile

fraction, so the gas-phase tar is more likely to volatilize during the process of pyrolysis or gasification.

Table 2. Elemental analysis of pine wood.

Carbon, C (%)	Hydrogen, H (%)	Oxygen, O (%)	Nitrogen, N (%)	Sulfur, S (%)
49.58	7.19	42.25	0.22	0.09

Table 3. Proximate analysis of pine wood.

Moisture, M (%)	Ash, A (%)	Volatile Fraction, V (%)	Fixed Carbon, FC (%)
7.65	1.67	78.10	12.55

N_2 was used as the reaction atmosphere for thermogravimetric analysis, and the volume flow rate was controlled between 40 mL/min and 50 mL/min. Pine wood particle was heated from T = 25 °C to T = 1100 °C at heating rate of V_T = 10 °C/min or V_T = 20 °C/min, respectively, (see Figures 5 and 6).

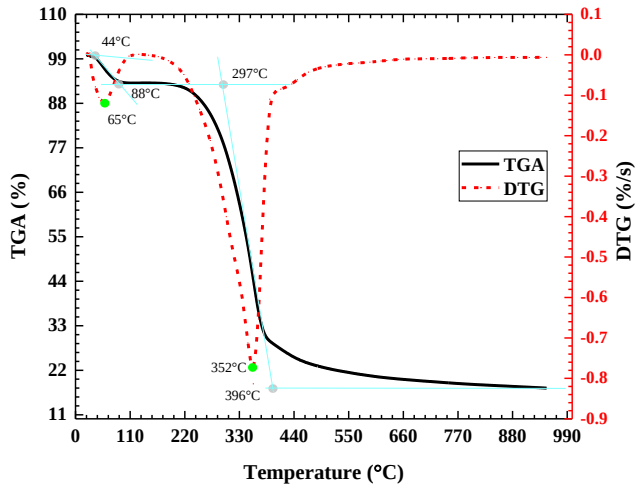

Figure 5. Thermogravimetric analysis results of pine wood under the condition of heating rate V_T = 10 °C/min.

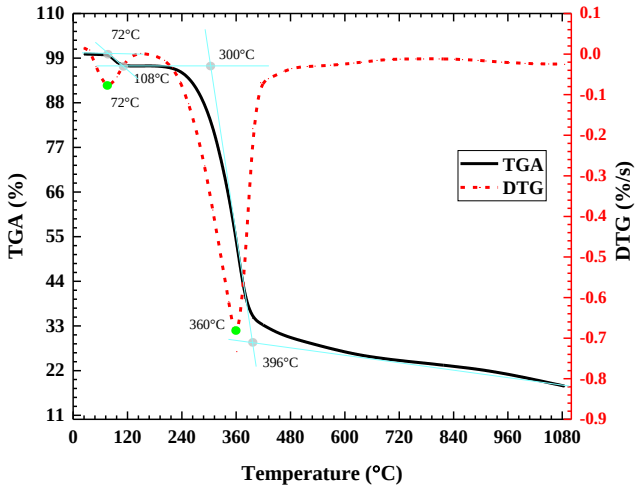

Figure 6. Thermogravimetric analysis results of pine wood under the condition of heating rate V_T = 20 °C/min.

At the heating rate of V_T = 10 °C/min, the water in pine wood particle began to separate out from T = 44 °C, and water evaporation ended when the temperature reached T = 88 °C. The evaporation rate reached the maximum at T = 65 °C. Volatile fraction began to release as the temperature raised to T = 297 °C. At temperature of T = 396 °C, fixed carbon and ash remained after volatile fractions were released. The release rate of volatile fraction is largest at T = 352 °C. In the temperature range of T = 297 °C~396 °C, mass-change rate of pine wood particle was 74.8%. At the heating rate of V_T = 20 °C/min, the majority of water in the pine wood particle began to evaporate at T = 72 °C. Water evaporation ended at T = 108 °C. At the temperature range of T = 300 °C~396 °C, volatile fraction was released gradually, and mass-change rate of pine wood particle was 68.2% at this temperature range. Volatile fraction was released at the largest rate at T = 360 °C. By comparing Figures 5 and 6, it can be found that the heating rate has little influence on the release of volatile fraction.

3.1.2. Gravimetric Analysis

- The total volume of the distilled sample was V_{TL}. The volume of sample injected into a dropping funnel was V_l at each time. The dripping speed was about 1 drop/s, and the distillation process took about 60 min. The condenser tube was kept cool during the process.
- The three-neck distillation flask (G_{bi}, tare weight) was below the dropping funnel. The three-neck distillation flask was placed in a constant temperature water bath, and the water bath temperature was 75 °C.
- The three-neck distillation flask was dried for 2 h and weighed, G_{bsi}. The least two parallel experiments ($V_{TL}/V_l = n \geq 2$) and one blank experiment were required for each tar sample. The blank experiment was performed via distilling dichloromethane, G_{empty} (tare weight).

The gas-phase tar content C in the pyrolysis process was obtained by the following calculation equation [24]:

$$C = M_{ka} \times V_{TL} \times \frac{T_{KN} + 273}{V_l \times V_{KN} \times 273} \quad (1)$$

$$V_{KN} = V_k \times t \quad (2)$$

In the Equations (1) and (2), C is the concentration of gas-phase tar, g·Nm^{-3}. M_{ka} is the residue mass of the solution sample to be tested after distillation, g. V_{TL} is the total volume of the sampled tar solution, mL. V_l is the volume of the parallel sample solution, mL. V_{KN} is the total volume of injected gas (nitrogen and Brown's gas) in a pyrolysis experiment, m^3. T_{KN} is the average temperature of gaseous product during the sampling, °C. V_k is the volume flow rate of gaseous products in the gas path IV, L/min. t is the pyrolysis time ($t = t_{end} - t_{start}$), min. t_{start} is the onset time, and t_{end} is the end time. The residue mass (M_{ka}) of the solution sample to be tested after distillation is calculated by the following equation.

$$M_{ka} = \frac{\sum\limits_{i=1\ldots n} (G_{bsi} - G_{bi})}{n} - G_{empty} \quad (3)$$

$$n = \frac{V_{TL}}{V_l} \quad (4)$$

In the Equations (3) and (4), G_{bsi} is the residue mass (with tare) after distillation in i group of parallel sample, g. G_{bi} is the weight of the distillation flask in the i group of parallel sample, g. n is the number of tested parallel samples in one experiment ($n \geq 2$). G_{empty} is the residue mass (without tare) after distillation in the blank experimental (dichloromethane, G_{empty} = 0.004 g).

In the experiment, if the volume flow rate of injected gas was too large, the gas-phase tar wasn't condensed completely, and if it was too small, the gas-phase tar could block the gas path. Therefore, before the formal experiment, it is necessary to determine the

appropriate volume flow rate of injected gas, V_k. According to the Figure 7, when the volume flow rate of mixed gas was V_k = 0.9 L/min, the absorption efficiency of gas-phase tar was better than other conditions. When the volume flow rate of mixed gas was small (V_k = 0.3 L/min), most of the gas-phase tar was attached to the inner wall of quartz tube. When the volume flow rate of mixed gas increased to V_k = 2.0 L/min, the gas-phase tar wasn't condensed completely. The precipitation of gas-phase tar decreased significantly, affecting the measurement results.

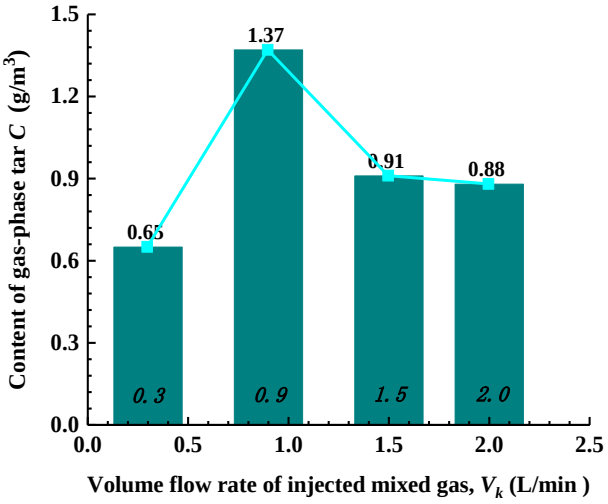

Figure 7. Influence of volume flow rate of injected mixed gas on the absorption efficiency of gas-phase tar.

Finally, the optimal volume flow rate of injected mixed gas for absorbing gas-phase tar was V_k = 0.9 L/min in the experiment. Secondly, parallel experiments were carried out for the gas-phase tar absorption capacity in each conical flasks, and the accuracy and repeatability of the experimental operation method were verified. In Figure 8, the No. 2 conical flask first absorbed gas-phase tar, and the gas-phase tar content is the largest. There is no significantly change of gas-phase tar content in No. 3, No. 4 and No. 5 conical flask. It is shown that the total absorbed amount of gas-phase tar differs by 1.4%, see Figure 8. Therefore, the experimental method in this paper can fully absorb gas-phase tar in pine wood particle pyrolysis.

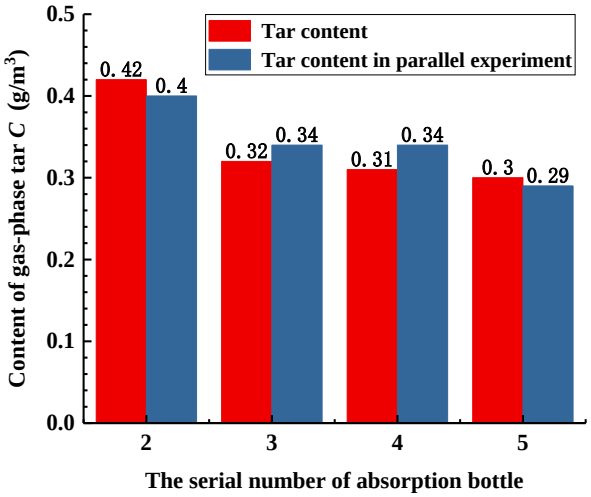

Figure 8. Absorption efficiency in the different conical flasks (No. 2, No. 3, No. 4 and No. 5) for gas-phase tar.

3.2. Results and Discussion

In the experiment, the volume flow rate of injected mixed gas was maintained at V_k = 0.92 L/min, and the flow volume ratio of Brown's gas to nitrogen was $X_{(Brown's\ gas)}$:N_2 = 1:100 = 1%, $X_{(Brown's\ gas)}$:N_2 = 5:100 = 5%, respectively. The effect of pyrolysis temperature on the gas-phase tar cracking and CO productive rate was studied experimentally under the condition with or without introduced Brown's gas. The lignin in the pine wood particle accounts for a large proportion, and lignin is the main source of gas-phase tar during the pyrolysis. As shown in Figure 9, in the initial stage of pine wood pyrolysis (T = 500 °C~700 °C), the gas-phase tar produced by the lignin pyrolysis is maintained at a relatively high level without the introduction of Brown's gas. At the same time, the content of gas-phase tar gradually decreases with the increasing pyrolysis temperature, because volatile fraction content is relatively large in the early stage of pine wood pyrolysis. The higher temperature facilitates the secondary cracking or polymerization between gas-phase tar and volatile fraction, thereby converting it into other gaseous products, chars, and some small or macromolecular liquid products. The content of gas-phase tar decreased from C = 67.76 g·Nm^{-3} to C = 57.14 g·Nm^{-3}, and the average cracking rate of gas-phase tar was $V_{(500°C\sim700°C)}$ = 5.31 g·Nm^{-3} for the increasing temperature per 1 °C.

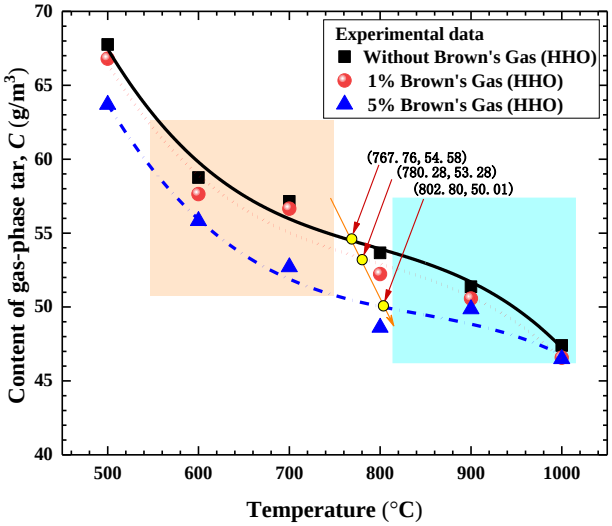

Figure 9. Variation of gas-phase tar with temperature.

When the pyrolysis temperature was in the range of T = 700°C~800°C, the gas-phase tar originating from cellulose pyrolysis began to be higher than that from lignin pyrolysis. Due to the small proportion of cellulose in pine wood, the cracking rate of gas-phase tar slowed down in this temperature range, and the content of gas-phase tar decreased from C = 57.14 g·Nm^{-3} to C = 53.66 g·Nm^{-3}. The average cracking rate of gas-phase tar was $V_{(700°C\sim800°C)}$ = 3.48 g/Nm^3°C with the increasing temperature per 1 °C. In the pyrolysis temperature range of 800 °C < T < 1000 °C, the cracking rate further slowed down, and the average cracking rate of gas-phase tar was $V_{(800\ °C\sim1000\ °C)}$ = 3.13 g·Nm $^{-3}$ with the increasing temperature per 1 °C. Under the condition of introduced Brown's gas, the gas-phase tar sustained accelerates cracking in the pyrolysis temperature range of T = 500 °C~800 °C, and the average cracking rate of gas-phase tar is $V_{(500°C\sim800°C)+(1\%)}$ = 4.8 g·Nm $^{-3}$ (X:N_2 = 1%) and $V_{(500°C\sim800°C)+(5\%)}$ = 5.02 g·Nm $^{-3}$ (X:N_2 = 5 %), respectively, for the increasing temperature per 1 °C. Therefore, with the increasing pyrolysis temperature, Brown's gas promotes the deep cracking of gas-phase tar, the average cracking rate of gas-phase tar is improved, and the thermochemical conversion rate is accelerated. In addition, Brown's gas lessens the energy barrier of thermochemical conversion for the gas-phase tar, and broadens the temperature range of gas-phase tar accelerated cracking, so the pyrolysis temperature required to cracking the same mass of gas-phase tar is lower.

From the Figure 10, under the condition without introduced Brown's gas, the CO content in the gaseous products increases due to the cracking of gas-phase tar with the increasing pyrolysis temperature. At the initial stage of pine wood pyrolysis (T = 500 °C ~600 °C), the CO volume fraction in the gaseous products began to increase slowly, and the production rate of CO was $V'_{(500°C\sim600°C)}$ = 1.37% for the increasing temperature per 1 °C. When the pyrolysis temperature was T> 600 °C (T = 600 °C~800 °C), due to the deep cracking of gas-phase tar and the partial reduction reaction between fixed carbon and water vapor in the flue gas, the volume fraction of CO in the gaseous products obviously increased. At the pyrolysis temperature of T = 800 °C, the CO volume fraction reached the maximum of 9.43%. Meanwhile, the production rate of CO was $V'_{(600°C\sim800°C)}$ = 1.87% with the increasing temperature per 1 °C. In the final stage of pine wood pyrolysis (800 °C < T< 1000 °C), the contribution of gas-phase tar cracking to CO formation was weakened, and the secondary reaction of carbon and water vapor became the main reason for CO formation. Therefore, the proportion of CO in gaseous products showed a slow downward trend. Under the condition of induced Brown's gas, the production rate of CO didn't change greatly for the increasing temperature per 1 °C in the initial stage of pine wood pyrolysis, and it maintained at the average level of $V'_{(500°C\sim600°C)+(1\%)}$ = 1.56% (X:N_2 = 1%)~$V'_{(500°C\sim600°C)+(5\%)}$ = 1.75% (X:N_2 = 5%). When the pyrolysis temperature was at the range of T = 600 °C~800 °C, the CO proportion in gaseous products continued to increase, and the largest volume fraction appeared at the pyrolysis temperature of T = 800 °C, the production rate of CO for the increasing temperature per 1 °C reached to $V'_{(600°C\sim800°C)+(1\%)}$ = 4.22% (X:N_2 = 1%) and $V'_{(600°C\sim800°C)+(5\%)}$ = 5.52% (X:N_2 = 5%), respectively. At the pyrolysis temperature of T = 900 °C ~1000 °C, the volume fraction of CO in gaseous products decayed rapidly, and the decay rate of CO with the increasing temperature per 1 °C was $V'_{(900°C\sim1000°C)+(1\%)}$ = 2.12% ($X_{(Brown's\ gas)}$:N_2 = 1 %) and $V'_{(600°C\sim800°C)+(5\%)}$ = 3.68% (X:N_2 = 5%), respectively. Therefore, while participating in the deep cracking of gas-phase tar, Brown's gas reduces the conversion energy barrier of gas-phase tar to CO, and improves the thermochemical conversion rate of gas-phase tar to CO. Meanwhile, in the high temperature pyrolysis stage, Brown's gas accelerates the further conversion of CO in gaseous products as the cracking rate of gas-phase tar slows down.

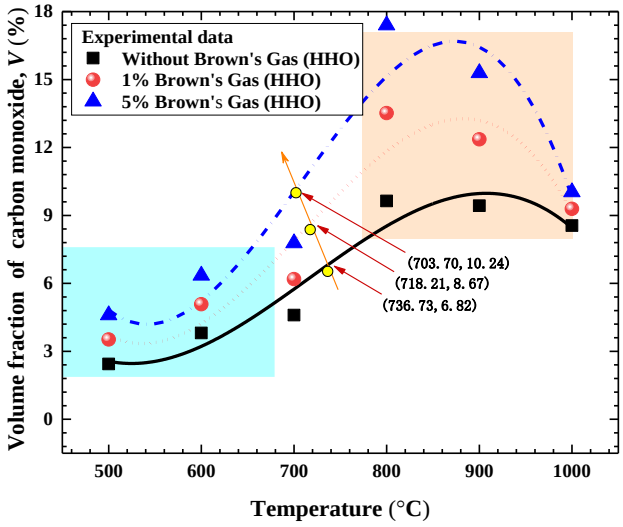

Figure 10. Variation of CO volume fraction with temperature.

In the Figure 11, at the same pyrolysis temperature, the cracking degree of gas-phase tar deepens with the increasing the flow volume ratio of Brown's gas to nitrogen. The pyrolysis temperature of pine wood was in the range of T = 500 °C~800 °C, and the content of gas-phase tar showed a significant downward trend with the increasing volume flow rate of Brown's gas.

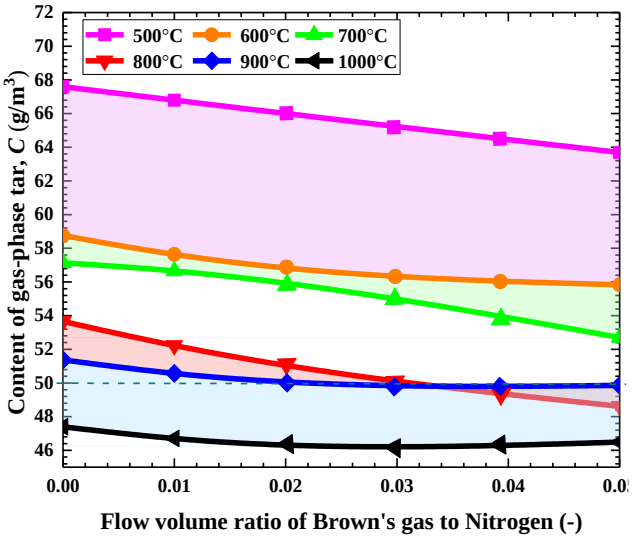

Figure 11. Relationship between the content of gas-phase tar and the flow volume ratio of Brown's gas to nitrogen in pine wood pyrolysis.

When the pyrolysis temperature was T = 800 °C, the cracking rate of gas-phase tar per unit flow volume ratio was largest, $V''_{800°C}$ = 3.62 (the cracking rate of gas-phase tar per unit flow volume ratio at other pyrolysis temperatures was $V''_{500°C}$ = 2.66, $V''_{600°C}$ = 1.55, $V''_{700°C}$ = 3.37, $V''_{900°C}$ = 0.60, $V''_{1000°C}$ = 1.07, respectively). As the pyrolysis temperature of T > 800 °C, the cracking rate of gas-phase tar changed little with the increasing Brown's gas concentration. Figure 12 shows the correspondence between the CO volume fraction and the flow volume ratio of Brown's gas to nitrogen. The increase of pyrolysis temperature is helpful to the thermochemical conversion of gas-phase tar, which directly leads to an increase in the overall production rate of CO. However, when the temperature was too high (T > 800 °C), the volume fraction of CO decreased, because the high pyrolysis temperature caused CO to react with the water vapor and hydrogen. When the pyrolysis temperature was T = 800 °C~900 °C, the improvement of CO production rate was the most obvious, caused by the increasing volume flow rate of Brown's gas, and the production rate of CO per unit flow volume ratio was $V''_{800°C}$ = 3.31 and $V''_{900°C}$ = 2.50, respectively (the production rate of CO per unit flow ratio of Brown's gas at other pyrolysis temperatures was $V''_{500°C}$ = 0.92, $V''_{600°C}$ = 1.09, $V''_{700°C}$ = 1.35, $V''_{1000°C}$ = 0.36, respectively).

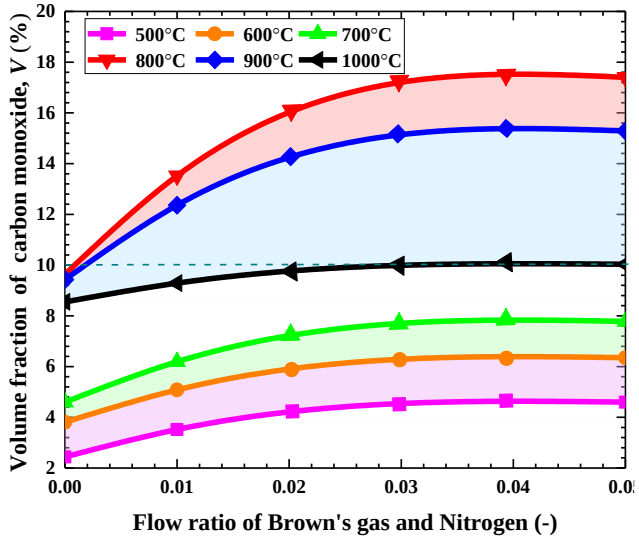

Figure 12. Relationship between the CO volume fraction and the flow volume ratio of Brown's gas to nitrogen in pine wood pyrolysis.

In summary, the increasing proportion of Brown's gas in the pyrolytic atmosphere at a certain temperature can effectively accelerate the gas-phase tar cracking. Based on the experimental results (see Table 4), the consumption of Brown's gas per 1 g/m^3 gas-phase tar cracking during the pine wood pyrolysis is quantitatively calculated.

Table 4. Parameters required for calculation.

The Flow Volume Ratio, (%)	Pyrolysis Temperature, (°C)	Volume Flow Rate of Brown's Gas, (mL/min)	Volume Flow Rate of Nitrogen, (L/min)	The Content of Gas-Phase Tar *C*, (g/m^3)	Residence Time, (min)
1	800	9.11	0.91	52.23	30
5	800	43.81	0.87	48.61	30

According to the ideal-gas equation of $PV = nRT$, the molar mass ratio of the gas is equal to the relative density ratio at the same temperature and pressure, and the density of Brown's gas ρ_{BG} can be calculated according to the following formula,

$$\frac{M_{BG}}{M_{N_2}} = \frac{\rho_{BG}}{\rho_{N_2}} \quad (5)$$

In the Equation (5), M_{BG} is the molar mass of Brown's gas, M_{BG} = 12.3 g/mol. M_{N2} is the molar mass of nitrogen. M_{N2} = 28 g/mol. ρ_{N2} is the nitrogen density, g/L. Therefore, the Brown's gas density is ρ_{BG} = 0.55 g/L. Within residence time of t = 30 min, the cracking mass of gas-phase tar is about 3.62 g/m^3, corresponding to the consumed mass of Brown's gas, which is $(V_{1\%BG}\text{-}V_{5\%BG}) \times t \times \rho_{BG}$ = 1.17 g. Therefore, the 0.32 m^3 Brown's gas is consumed per 1 g·Nm $^{-3}$ gas-phase tar cracking.

As shown in Figure 13, when the flow volume ratio of Brown's gas to nitrogen was 1%, the gas-phase tar gradually cracked with the increasing the pyrolysis temperature, and the CO volume fraction first increased and then decreased. When the temperature was up to T = 800 °C, the volume fraction of CO reached the maximum value, $V_{800°C}$ = 13.52%. Correspondingly, the distribution of gaseous product temperature (T_{KN}) showed a monotonous upward trend, but the variation of temperature rise rate was opposite to that of cracking rate of gas-phase tar. In the pyrolysis temperature range of T = 500 °C~750 °C, the cracking rate of gas-phase tar was relatively large, and the cleavage of carbonyl-bond in gas-phase tar was the main source of CO. In this process, it absorbed the heat in the environment, resulting in the slowed down rise rate of gaseous product temperature (T_{KN}). When the pyrolysis temperature was higher than T = 750 °C, the cracking rate of gas-phase tar decreased and the rise rate of gaseous product temperature (T_{KN}) increased.

Therefore, the turning point of acceleration and deceleration of CO production rate was located at the pyrolysis temperature of T = 750 °C. From the Figure 14, when the volume flow rate of Brown's gas increased, the overall average level of gas-phase tar content and gaseous product temperature (T_{KN}) decreased, and the overall level of CO volume fraction increased significantly. Compared with the Figure 13, the rise rate of gaseous product temperature (T_{KN}) decreased obviously. In the pyrolysis temperature range of T = 500 °C~700 °C, the cracking rate of gas-phase tar was larger, while the rise rate of gaseous product temperature (T_{KN}) was smaller. When the pyrolysis temperature was T > 700 °C, the cracking rate of gas-phase tar decreased, while the rise rate of gaseous product temperature (T_{KN}) increased. The turning point of the acceleration and deceleration of CO production rate was located at the pyrolysis temperature of T = 700 °C, and the position of turning point moved forward with the increasing the flow volume ratio of Brown's gas to nitrogen.

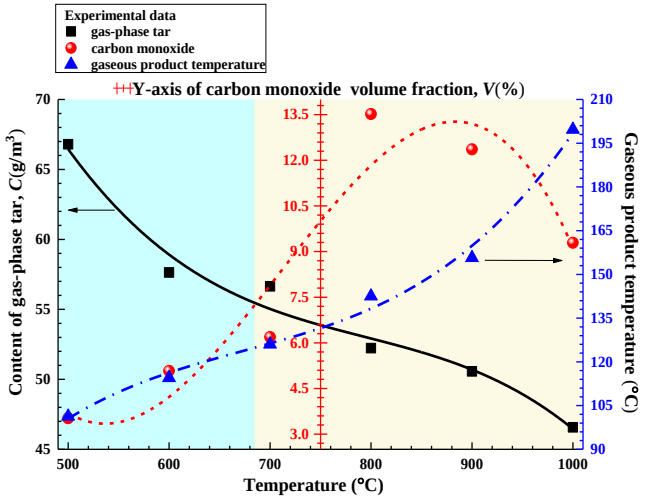

Figure 13. Variation of gas-phase tar content, CO volume fraction, and gaseous product temperature with the pyrolysis temperature under the flow volume ratio of Brown's gas to nitrogen of 1%.

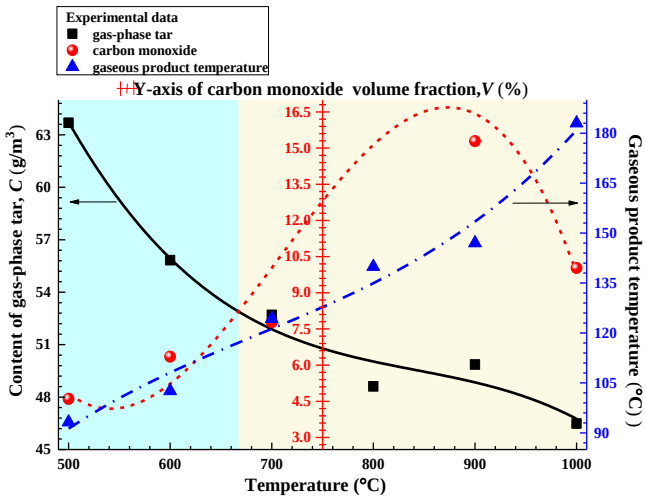

Figure 14. Variation of gas-phase tar content, CO volume fraction, and gaseous product temperature with the pyrolysis temperature under the flow volume ratio of Brown's gas to nitrogen of 5%.

Figure 15 shows the equilibrium relationship between the flow volume ratio of Brown's gas to nitrogen, gas-phase tar content, gaseous product temperature, and CO volume fraction during the pine wood pyrolysis. Obviously, in order to achieve a lower gas-phase tar content, a higher pyrolysis temperature is required without introduced the Brown's gas (the flow volume ratio of Brown's gas to nitrogen is X:N_2 = 0%). Biomass gas-phase tar reaches lower content after primary cracking and secondary cracking, as shown in Figure 15a. With the increasing the volume flow rate of Brown's gas, a wider selection space is provided for the content balance among the gas-phase tar content, gaseous product temperature, and CO volume fraction, (see the zone surrounded by solid lines in the Figure 15d–f). Meanwhile, a certain pyrolysis condition of a small gas-phase tar content and a large CO volume fraction can be obtained at the lower pyrolysis temperature, (see the zone enclosed by dotted line in Figure 15f). Therefore, based on the experimental conditions in this paper, the minimum gas-phase tar content and the maximum CO volume fraction are obtained at the pyrolysis temperature of 800 °C and the flow volume ratio of Brown's gas to nitrogen of 5%. This provides some guidance for further pilot scale experiments.

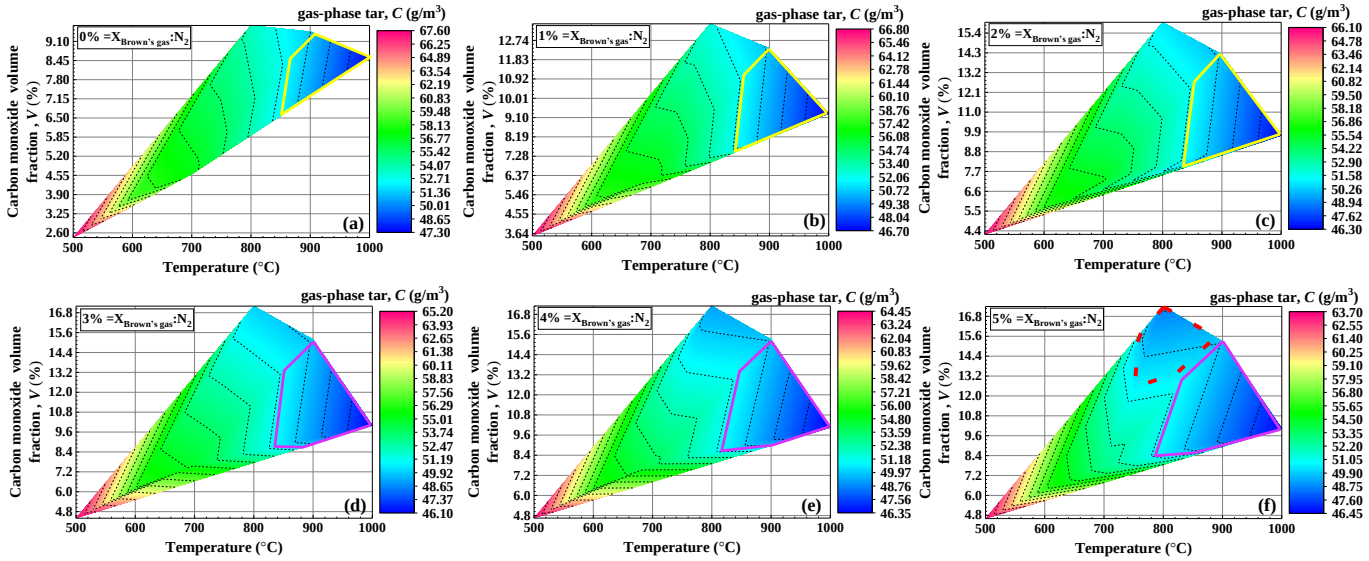

Figure 15. Equilibrium relationship between the flow volume ratio of Brown's gas to nitrogen, gas-phase tar content, gaseous product temperature, and CO volume fraction. (**a**) $X_{Brown's\ Gas:}N_2$ = 0%, (**b**) $X_{Brown's\ Gas:}N_2$ = 10%, (**c**) $X_{Brown's\ Gas:}N_2$ = 20%, (**d**) $X_{Brown's\ Gas:}N_2$ = 30%, (**e**) $X_{Brown's\ Gas:}N_2$ = 40%, (**f**) $X_{Brown's\ Gas:}N_2$ = 50%.

4. Conclusions

- Under the condition of introduced Brown's gas, the temperature range of gas-phase tar accelerated cracking is extended from Tv = 500 °C~700 °C to T = 500 °C ~800 °C. The average cracking rate of gas-phase tar for the increasing temperature per 1 °C increases from the original $V_{(500°C\sim800°C)}$ = 4.58 g·Nm $^{-3}$ ($X_{(Brown's\ gas)}$:N_2 = 0%) to the $V_{(500°C\ 800°C)+(1\%)}$ = 4.8 g·Nm $^{-3}$ (X:N_2 = 1%) and $V_{(500°C\sim800°C)+(5\%)}$ = 5.02 g·Nm $^{-3}$ (X:N_2 = 5%). Therefore, Brown's gas reduces the energy barrier of thermochemical conversion for gas-phase tar and broadens the temperature range of gas-phase tar accelerated cracking. In addition, the rich active radicals in Brown's gas increase the thermochemical conversion rate of gas-phase tar.
- Under the condition of introduced Brown's gas, the effect of Brown's gas on the CO production rate is not obvious in the initial stage of pine wood pyrolysis (T = 500 °C~600 °C), and the CO production rate for increasing temperature per 1 °C is maintained at the range of $V'_{(500°C\sim600°C)+(1\%)}$ = 1.56% (X:N_2 = 1%)~$V'_{(500°C\sim600°C)+(5\%)}$ = 1.75% (X:N_2 = 5%). When the pyrolysis temperature is at range of T = 600 °C~800 °C, the Brown's gas has a significant effect on the production rate of CO, and the largest CO volume fraction appears at the pyrolysis temperature of T = 800 °C. The CO production rate for the increasing temperature per 1 °C increases from the original $V'_{(600°C\sim800°C)}$ = 1.87% (X:N_2 = 0%) to $V'_{(600°C\sim800°C)+(1\%)}$ = 4.22% (X:N_2 = 1%) and $V'_{(600°C\sim800°C)+(5\%)}$ = 5.52% (X:N_2 = 5%). Therefore, while participating in the deep cracking of gas-phase tar, Brown's gas reduces the conversion energy barrier of gas-phase tar to CO and improves the thermochemical conversion rate of gas-phase tar to CO.
- The distribution of gaseous product temperature in the pine wood pyrolysis presents a monotonically rising trend, but the changing trend of gaseous product temperature is opposite to that of the gas-phase tar cracking rate. In the pyrolysis temperature range of T = 500 °C~750 °C, the cracking rate of gas-phase tar is relatively large, and the cleavage of carbonyl-bond of gas-phase tar is the main source of CO generation. In this process, the heat in the environment is absorbed, resulting in a slow rise rate of gaseous product temperature (T_{KN}).

Author Contributions: Project administration, S.Y.; investigation, Y.F.; writing—original draft preparation, J.C.; investigation, Z.L.; writing—review and editing, D.Q.; formal analysis, L.X.; methodology, Y.X. All authors have read and agreed to the published version of the manuscript.

Funding: The present work is supported financially by the Science and Technology Program Foundation of Liaoning Province (2021-MS-270 and LJKZ1109), Shenyang Science and Technology Project (No. 21-108-9-08 and No. RC210010).

Conflicts of Interest: The authors declare no conflict of interest.

Appendix A

Table A1. Elementary reactions and chemical reaction kinetic parameters related to the C_6H_6 [25].

Elementary Reaction	Pre-Exponential Factor, A_0 ($cm^3 \cdot mol^{-1} \cdot s^{-1}$)	Temperature Index, m (-)	Activation Energy, E_0 ($kcal \cdot mol^{-1}$)
$C_6H_6 + O_2 = C_6H_5 + HO_2$	6.30×10^{13}	0.0	60,000.0
$C_6H_6 + OH = C_6H_5 + H_2O$	1.63×10^{8}	1.42	1454.0
$C_6H_6 + OH = C_6H_5OH + H$	6.70×10^{12}	0.0	10,592.0
$C_6H_6 + O = C_6H_5O + H$	2.40×10^{13}	0.0	4670.0
$C_6H_6 + H = C_6H_5 + H_2$	3.03×10^{2}	3.3	5690.0

Table A2. Elementary reactions and chemical reaction kinetic parameters related to the $C_6H_5CH_3$ [25].

Elementary Reaction	Pre-Exponential Factor, A_0 ($cm^3 \cdot mol^{-1} \cdot s^{-1}$)	Temperature Index, m (−)	Activation Energy, E_0 ($kcal \cdot mol^{-1}$)
$C_6H_5OH + OH = C_6H_5O + H_2O$	2.95×10^{6}	2.0	−1310.0
$C_6H_5OH + CH_3 = C_6H_5O + CH_4$	1.81×10^{11}	0.0	7716.0
$C_6H_5OH + H = C_6H_5O + H_2$	1.58×10^{13}	0.0	6100.0
$C_6H_5OH + O = C_6H_5O + OH$	2.81×10^{13}	0.0	7352.0
$C_6H_5OH + C_2H_3 = C_2H_4 + C_6H_5O$	6.00×10^{12}	0.0	0.0
$C_6H_5OH + C_6H_5 = C_6H_6 + C_6H_5O$	4.91×10^{12}	0.0	4400.0

Table A3. Elementary reactions and chemical reaction kinetic parameters related to the C_7H_8 [25].

Elementary Reaction	Pre-Exponential Factor, A_0 ($cm^3 \cdot mol^{-1} \cdot s^{-1}$)	Temperature Index, m (−)	Activation Energy, E_0 ($kcal \cdot mol^{-1}$)
$C_6H_5CH_3 = C_6H_5 + CH_3$	1.40×10^{16}	0.0	99,800.0
$C_6H_5CH_3 + O_2 = C_6H_5CH_2 + HO_2$	2.00×10^{12}	0.0	39,080.0
$C_6H_5CH_3 + OH = C_6H_5CH_2 + H_2O$	1.26×10^{13}	0.0	2583.0
$C_6H_5CH_3 + O = C_6H_5CH_2 + OH$	5.00×10^{8}	1.5	8000.0
$C_6H_5CH_3 + H = C_6H_5CH_2 + H_2$	3.98×10^{2}	3.44	3120.0
$C_6H_5CH_3 + O = OC_6H_4CH_3 + H$	1.63×10^{13}	0.0	3418.0
$C_6H_5CH_3 + CH_3 = CH_4 + C_6H_5CH_2$	3.16×10^{11}	0.0	9500.0
$C_6H_5CH_3 + C_6H_5 = C_6H_6 + C_6H_5CH_2$	2.10×10^{12}	0.0	4400.0
$C_6H_5CH_3 + H = C_6H_6 + CH_3$	1.20×10^{13}	0.0	5148.0

Table A4. Elementary reactions and chemical reaction kinetic parameters related to the $C_{10}H_7CH_3$ [25].

Elementary Reaction	Pre-Exponential Factor, A_0 ($cm^3 \cdot mol^{-1} \cdot s^{-1}$)	Temperature Index, m (−)	Activation Energy, E_0 ($kcal \cdot mol^{-1}$)
$C_{10}H_7CH_3 + OH = C_{10}H_7CH_2 + H_2O$	1.27×10^{13}	0.0	2583.0
$C_{10}H_7CH_3 + O^- = C_{10}H_7CH_2 + OH$	5.00×10^{8}	1.5	8000.0
$C_{10}H_7CH_3 + H = C_{10}H_7CH_2 + H_2$	3.98×10^{2}	3.44	3120.0
$C_{10}H_7CH_3 + H = C_{10}H_8 + CH_3$	1.20×10^{13}	0.0	5148.0

Table A5. Elementary reactions and chemical reaction kinetic parameters related to the $CH_3C_6H_4CH_3$ [25].

Elementary Reaction	Pre-Exponential Factor, A_0 ($cm^3 \cdot mol^{-1} \cdot s^{-1}$)	Temperature Index, m (−)	Activation Energy, E_0 ($kcal \cdot mol^{-1}$)
$CH_3C_6H_4CH_3 + OH = CH_3C_6H_4CH_2 + H_2O$	2.95×10^{13}	0.0	2623.0
$CH_3C_6H_4CH_3 + O = CH_3C_6H_4CH_2 + OH$	5.00×10^{8}	1.5	8000.0
$CH_3C_6H_4CH_3 + H = CH_3C_6H_4CH_2 + H$	3.98×10^{2}	3.44	3120.0

References

1. Capurso, T.; Stefanizzi, M.; Torresi, M.; Camporeale, S.M. Perspective of the role of hydrogen in the 21st century energy transition. *Energy Convers. Manag.* **2022**, *251*, 114898. [CrossRef]
2. Arsalis, A.; Papanastasiou, P.; Georghiou, G.E. A comparative review of lithium-ion battery and regenerative hydrogen fuel cell technologies for integration with photovoltaic applications. *Renew. Energy* **2022**, *191*, 943–960. [CrossRef]
3. Ajiwibowo, M.W.; Darmawan, A.; Huda, M.; Surjosatyo, A.; Aziz, M. Integrated power-to-gas and power generation system through chemical looping combustion: A conceptual design. *Energy Procedia* **2019**, *158*, 1904–1909. [CrossRef]
4. Soly, A.; Kady, M.; Farrag, A.; Gad, M.S. Comparative experimental investigation of oxyhydrogen (HHO) production rate using dry and wet cells. *Int. J. Hydrogen Energy* **2021**, *46*, 12639–12653. [CrossRef]
5. Baltacolu, M.K. A novel application of pulse width modulation technique on hydroxy gas production. *Int. J. Hydrogen Energy* **2019**, *44*, 9726–9734. [CrossRef]
6. Streblau, M.; Aprahamian, B.; Dechev, A.; Dimov, D. Investigation of the influence of the electric current's magnitude on the operating regime of an oxyhydrogen generator. In Proceedings of the Conference: Practical Energy Prblems and Trends in Efficient Technologies (PEP TET 2013), Sofia, Bulgaria, 22 September 2013; Volume 48, pp. 5–6.
7. Kady, M.; Farrag, A.; Gad, M.S.; Soly, A.; Hashish, H. Parametric study and experimental investigation of hydroxy (HHO) production using dry cell. *Fuel* **2020**, *282*, 118825. [CrossRef]
8. King, M.B. Water Electrolyzers and the Zero-Point Energy. *Phys. Procedia* **2011**, *20*, 435–445. [CrossRef]
9. Paparao, J.; Murugan, S. Oxy-hydrogen gas as an alternative fuel for heat and power generation applications—A review. *Int. J. Hydrogen Energy* **2021**, *46*, 37705–37735. [CrossRef]
10. Butt, O.M.; Ahmad, M.S.; Che, H.S.; Rahim, N.A. Usage of on-demand oxyhydrogen gas as clean/renewable fuel for combustion applications: A review. *Int. J. Green Energy* **2021**, *18*, 1405–1429. [CrossRef]
11. Arjun, T.B.; Atul, K.P.; Muraleedharan, A.P.; Walton, P.A.; Raj, A.A. A review on analysis of HHO gas in IC engines. *Mater. Today Proc.* **2019**, *11*, 1117–1129. [CrossRef]
12. Gad, M.S.; El-Fakharany, M.K.; Elsharkawy, E.A. Effect of HHO gas enrichment on performance and emissions of a diesel engine fueled by biodiesel blend with kerosene additive. *Fuel* **2020**, *280*, 118632. [CrossRef]
13. Gad, M.S.; Razek, S. Impact of HHO produced from dry and wet cell electrolyzers on diesel engine performance, emissions and combustion characteristics. *Int. J. Hydrogen Energy* **2021**, *46*, 22277–22291. [CrossRef]
14. Liu, S.; Zhang, L.B.; Wang, Z.; Hua, L.; Zhang, Q.S. Investigating the combustion stability of shale gas engines under HHO. *Fuel* **2021**, *291*, 120098. [CrossRef]
15. Hyun, J.S.; Park, J.W.; Maken, S.; Park, J.J. Vitrification of fly and bottom ashes from municipal solid waste incinerator using Brown's Gas. *J. Ind. Eng. Chem.* **2004**, *10*, 361–367.
16. Maken, S.; Jang, S.H.; Park, J.W.; Song, H.C.; Lee, S.; Chang, E.H. Vitrification of MSWI fly ash using Brown's gas and fate of heavy metals. *J. Sci. Ind. Res. India* **2005**, *64*, 198–204.
17. Park, K.; Hyun, J.; Maken, S.; Jang, S.; Park, J.W. Vitrification of municipal solid waste incinerator fly ash using brown's gas. *Energy Fuel* **2005**, *19*, 258–262. [CrossRef]
18. Min, S.Y.; Maken, S.; Park, J.W.; Gaur, A.; Hyun, J.S. Melting treatment of waste asbestos using mixture of hydrogen and oxygen produced from water electrolysis. *Korean J. Chem. Eng.* **2008**, *25*, 323–328. [CrossRef]
19. Wang, C.N.; Chou, M.T.; Hsu, H.P.; Wang, J.W.; Selvaraj, S. The efficiency improvement by combining HHO gas, coal and oil in boiler for electricity generation. *Energies* **2017**, *10*, 251. [CrossRef]
20. Kenanolu, R.; Baltaciolu, E. An experimental investigation on hydroxy (HHO) enriched ammonia as alternative fuel in gas turbine. *Int. J. Hydrogen Energy* **2020**, *46*, 29638–29648. [CrossRef]
21. Gu, X.S.; Cheng, M.L.; Zhang, X.F.; Zeng, Y. The pollutant discharge improvement by introducing HHO gas into biomass boiler. *confirm Int. J. Hydrogen Energy* **2021**, *46*, 23292–23300. [CrossRef]
22. Nabil, T.; Dawood, M.M.K. Enabling efficient use of oxyhydrogen gas (HHO) in selected engineering applications; transportation and sustainable power generation. *J. Clean Prod.* **2019**, *237*, 117798. [CrossRef]
23. Lobo, L.Q.; Ferreira, A.G.M. Phase equilibria from the exactly integrated Clapeyron equation. *J. Chem. Thermodyn.* **2001**, *33*, 1597–1617. [CrossRef]

24. Simell, P.; Stahlberg, P.; Kurkela, E. Provisional protocol for the sampling and anlaysis of tarand particulates in the gas from large-scale biomass gasifiers. Version 1998. *Biomass Bioenergy* **2000**, *18*, 19–38. [CrossRef]
25. Adapted from NIST Chemistry WebBook. Standard Reference Database the Number 69. The U.S. Secretary of Commerce on Behalf of the United States of America. Available online: https://webbook.nist.gov/chemistry/name-ser/[EO/OL] (accessed on 1 January 2022).